Materials Science inc. Nanomaterials & Polymers

Ag-Nanoparticles-Decorated Ge-Nanowhisker Grafted on Carbon Fiber Cloth as Flexible and Effective SERS Substrates

Jing Liu,[a, b, e] Chuhong Zhu,[a] Qijun Pan,[a, c] Guowen Meng,*[a, c] and Yong Lei[d]

Three-dimensional (3D) flexible surface enhanced Raman scattering (SERS) substrates of silver nanoparticles (Ag-NPs) decorated Germanium nanowhiskers (Ge-NWHKs) grafted on carbon fiber cloth (CFC) (denoted as Ag-NPs@Ge-NWHKs@CFC) are constructed *via* chemical vapor deposition growth of high-density Ge-NWHKs on CFC and then assembly of Ag-NPs on the Ge-NWHKs by galvanic displacement. Ordered 3D framework of Ge-NWHKs grafted flexible CFC impels the formation of large amounts of Ag-NPs with homogenous distribution *via* spontaneous reduction of Ag^+ ions. Thus, the Ag-NPs@Ge-NWHKs@CFC SERS substrates present ultra-high sensitivity, good reproducibility, and high flexibility. This SERS sensor has achieved a detection limit of 1 pM for Rhodamine **6**G and 0.1 nM for thiram respectively. The as-fabricated SERS substrates show promising potential for applications in rapid detection of trace organic pollutants in the aquatic environment.

1. Introduction

Surface enhanced Raman scattering (SERS), as a rapid, highly sensitive and non-destructive method for fingerprint detection, has been widely used in chemical and biochemical analysis.[1–7] To carry out perfect SERS measurement, SERS substrates are supposed to not only have high-density "hot spots" with highly concentrated electromagnetic (EM) field to make a significant contribution to the Raman signal enhancement, but also have good uniformity to guarantee reproducible SERS measurements.[8–14] Since ordered three-dimensional (3D) micro/nanostructures (mainly plasmonic nanoparticles) with large surface area can support high-density "hot spots" while ensuring a good uniformity, various SERS substrates of noble metal nanoparticles (NPs) decorated 3D nanostructures were constructed,[15–18] such as Ag-NPs@ZnO nanowire arrays,[19] Ag-NPs@vertical graphene-nanosheet,[20] Ag-nanocubes@photolithographic microstructures and Pt@TiO_2 nanotube arrays.[21–22] In particular, flexible 3D nanostructures are more desirable for constructing SERS substrates, because of the fragile and inconvenience performance of traditional rigid templates.[23–26] For example, gold nanoplates (Au-nanoplates) were grafted onto carbon-nanotube sheets by hydrothermal reduction process to achieve flexible SERS substrates.[27] Also, Ag-NPs were decorated on PAN nanohump arrays or Au-NPs were assembled onto free-standing Si-nanowire paper *via* sputtering.[28–29] However, these reported methods of bonding Ag-NPs to flexible nanostructures are expensive and/or complex, where expensive instruments or reducing agents are used, and restricting their popularity.

Galvanic displacement, which depends on the potential difference between substrates and metal ions, has become a popular method for synthesizing metal nanoparticles, due to its low cost and easy operation.[30] Ag-nanostructures were facilely synthesized right before SERS detection by galvanic displacement method so that the oxidization of Ag can be avoided and the high SERS sensitivity can be guaranteed. Germanium (Ge) with the capability of reducing Ag^+ and $AuCl_4^-$ spontaneously *via* galvanic displacement has been applied in the fabrication of SERS substrates.[31] For example, Ag-NPs were decorated on Ge nanowires or Ge wafers through galvanic displacement to obtain highly sensitive SERS substrates.[32–33] We also constructed Ag-NPs-decorated Ge-nanowhiskers (Ge-NWHKs) grafted on Si-micropillars which present both ultra-high sensitivity and good reproducibility.[34] However, all these SERS substrates are rigid, which are not conducive in some applications, that need flexible and bendable substrates. For example, analytes on irregular surfaces are difficult to detect with rigid substrates, but can be loaded and tested by

[a] *Dr. J. Liu, Dr. C. Zhu, Q. Pan, Prof. G. Meng*
Key Laboratory of Materials Physics CAS Center for Excellence in Nanoscience Anhui Key Laboratory of Nanomaterials and Nanotechnology
Institute of Solid State Physics Chinese Academy of Sciences
Hefei 230031, P. R. China
E-mail: gwmeng@issp.ac.cn
[b] *Dr. J. Liu*
University of Chinese Academy of Sciences
Beijing 100049, P. R. China
[c] *Q. Pan, Prof. G. Meng*
Department of Materials Science & Engineering
University of Science and Technology of China
Hefei 230026, P. R. China
[d] *Prof. Y. Lei*
Institut für Physik & IMN MacroNano@ (ZIK)
Technische Universität Imenau
Ilmenau 98693, Germany
[e] *Dr. J. Liu*
China Star Optoelectronics Technology Co., Ltd,
Shenzhen 518800, P. R. China

Supporting information for this article is available on the WWW under https://doi.org/10.1002/slct.202001290

swabbing it with flexible SERS substrates.[35–36] Also, wearable sensors need to be flexible.[37]

Herein, we report a simple large-scale synthetic approach for flexible 3D SERS substrates made of Ag-NPs decorated Ge-NWHKs grafted on carbon fiber cloth (CFC), denoted as Ag-NPs@Ge-NWHKs@CFC, with high sensitivity and good reproducibility. The CFC is promising as flexible materials and has wide application and development prospects due to its low cost, fatigue and corrosion resistance.[38] The fabrication procedure of flexible 3D SERS substrates based on CFC is shown in Figure 1. Firstly, CFC was immersed in a mixed solution of graphene oxide (GO) and nickel nitrate ($Ni(NO_3)_2$) to effectively decorate the catalyst precursor $Ni(NO_3)_2$ and GO on the surface of each carbon fiber. Then, flocky Ge-NWHKs were grafted on CFC *via* chemical vapor deposition (CVD) in a mixed gas of germane (GeH_4) and hydrogen (H_2). Finally, Ag-NPs were decorated onto the Ge-NWHKs by immersing the Ge-NWHKs grafted CFC in an aqueous solution of silver nitrate ($AgNO_3$) for a few minutes. The fabrication approach and the resultant Ag-NPs@Ge-NWHKs@CFC SERS substrates have the following advantages. Firstly, substantial amounts of Ag-NPs are evenly distributed on the ordered 3D nanostructures of Ge-NWHKs@CFC, leading to high SERS activity and good SERS-signal reproducibility. Secondly, galvanic displacement requiring no reducing agents and expensive instruments shall be a green and facile way to decorate Ag-NPs on the 3D-frameworks. Thirdly, based on CFC with good durability and flexibility, the 3D SERS substrates can be easily tailored into many desired shapes for practical applications. As an application demonstration, the Ag-NPs@Ge-NWHKs@CFC SERS substrates are utilized for probing Rhodamine **6**G (R6G) and thiram (a fungicide), and have achieved a maximum detection of 1 pM and 0.1 nM for R6G and thiram respectively, showing promising potential in SERS-based rapid detection of trace organic pollutants in environment.

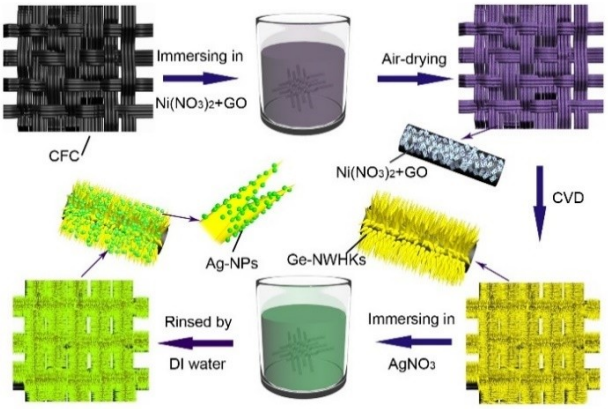

Figure 1. Schematic for the synthesis of Ag-NPs@Ge-NWHKs@CFC.

2. Results and Discussion

After CVD growth of Ge-NWHKs on CFC, Ge-NWHKs grafted CFC was obtained, as shown in Figure 2. Scanning electron microscopy (SEM) observations reveal that large amounts of Ge-NWHKs with average length of about 2 μm were homogenously distributed on CFC (Figure 2a, b, c). The cross-sectional image of Ge-NWHKs in Figure 2c shows that the diameters were about 500 nm and 250 nm at the bottom and the middle of Ge-NWHKs respectively. The immersion of CFCs in the aqueous solution of $Ni(NO_3)_2$ and GO took an important role in the growth of dense and uniform Ge-NWHKs. The Ni^{2+} adsorbed on CFCs were later reduced in H_2 at 330 °C and converted into Ni nanoparticles, which acted as catalyst to form Ni–Ge eutectic alloy in GeH_4. When the alloy was supersaturated, Ge nanocrystals nucleated and formed Ge substance.[34,39] With the Ni nanoparticles gradually integrating into Ge, an evolution of Ge morphology changing from nanofilm to needle-like nanowhisker was observed (Figure 2c). The lattice-resolved TEM image (Figure 2d) of the Ge-NWHK shows clear lattice fringes, demonstrating the crystalline nature of the Ge-NWHK.[40] It is worth to mention that the hydrophilic functional groups (–COOH, –C=O, and –OH) on the surface of GO are essential for immobilizing sufficient Ni^{2+} onto CFCs.[41–42] Without GO, only few Ge NWHKs with smaller size (about 0.5 μm in length) were grown onto the CFC unevenly (Figure S1, Supporting Information).

Then Ag-NPs were assembled on Ge-NWHKs (Figure 2a-c) through galvanic displacement. Different standard reduction potentials of Ge and Ag are given as below,

$$Ag^{+} + e^{-} \leftrightharpoons Ag \quad E_0 = 0.799\,V$$

$$Ge^{4+} + 4e^{-} \leftrightharpoons Ge \quad E_0 = 0.124\,V$$

Ag has a higher standard reduction potential than that of Ge, leading to the spontaneous formation of Ag-NPs when Ag^{+} ions come in contact with Ge. For the deposition of Ag-NPs, Ge-NWHKs grafted CFC was immersed in an aqueous solution of $AgNO_3$. Since electromagnetic fields increase dramatically with the narrowing of the junctions of Ag-NPs,[43–44] it is important to optimize their distribution by controlling the $AgNO_3$ immersion time. As shown in Figure 3a, after 3 mins of $AgNO_3$ immersion, small Ag-NPs (with diameters less than 20 nm) were sparsely assembled on the Ge-NWHKs, where the average gap between the neighboring Ag-NPs is about 33 nm. The above-mentioned diameters and average gap size of Ag-NPs were obtained from the size distribution and the junction size distribution of Ag-NPs in Figure 3a (shown in Figure S2b and c, Supporting Information). With the immersion duration increases to 9 mins, the SEM image (shown in Figure 3b) shows that from the Ge-NWHK root towards the Ge-NWHK tip, Ag-NPs become larger and larger and tend to aggregate. This is due to the larger curvature and higher surface free energy on the top of Ge-NWHK. The reaction of galvanic displacement undergoes fast at the position with higher surface free energy, leading to the formation of larger Ag-NPs. The corresponding size and

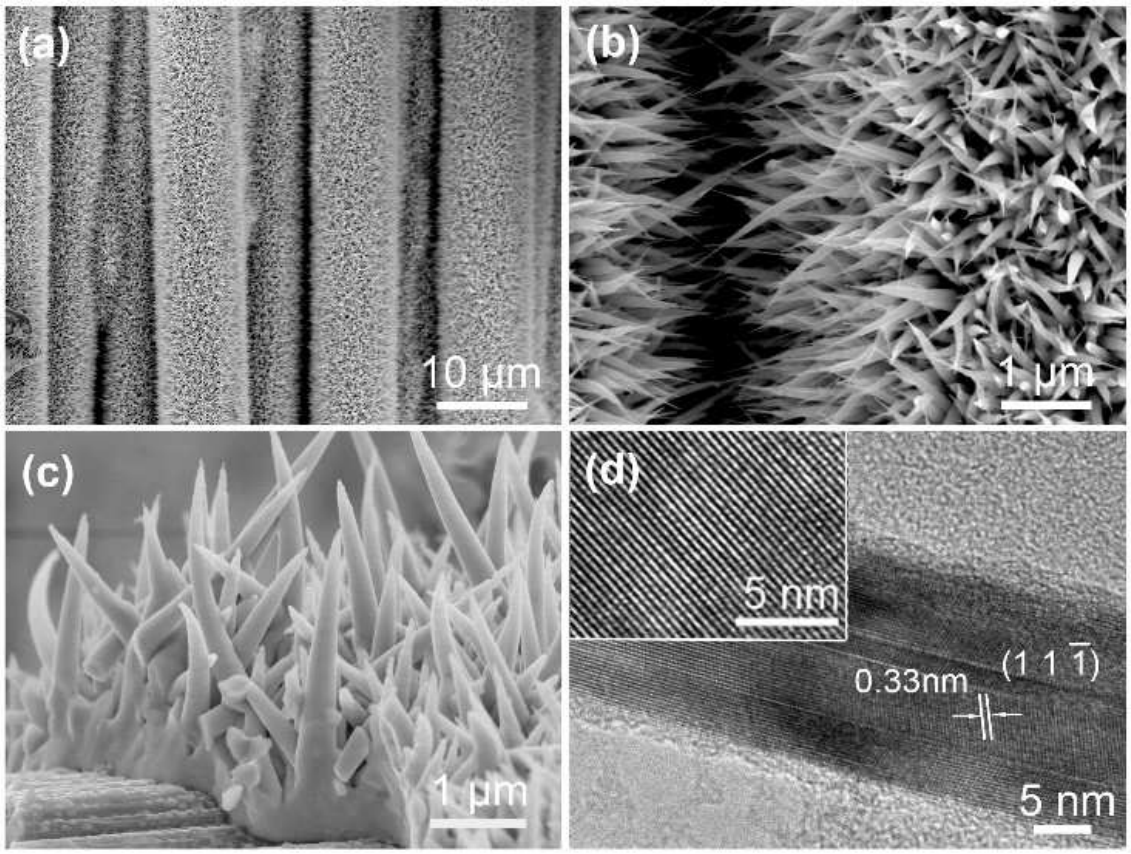

Figure 2. (a, b) SEM views of the Ge-NWHKs grafted on CFC with different magnifications. (c) cross-sectional view of the Ge-NWHKs and (d) TEM view of a Ge-NWHK.

gap size distribution of Ag-NPs (shown in Figure S2e and f) reveal that most of the Ag-NPs grow to about 20 nm and most of the gaps between the neighboring Ag-NPs decrease to about 10 nm (Figure 3b). There exist large amounts of "hot spots" appearing in such gaps. Further elongating the immersion duration to 12 mins, bulk Ag nanostructures with larger volumes were covered onto the Ge-NWHKs and lots of gaps disappeared (Figure 3c). The formation of Ag-NPs was confirmed by energy dispersive X-ray spectroscopy (EDS) (Figure 3d) on Ag-NPs@Ge-NWHKs with the immersion duration of 9 mins (the inset shows the SEM image of the corresponding Ag-NPs@Ge-NWHKs). Higher resolution SEM image of Ag-NPs@Ge-NWHK (Figure S3 in Supporting Information) further verifies the existence of high density "hot spots" on the fabricated SERS substrate. The optical absorption spectra of Ge-NWHKs@CFC and Ag-NPs@Ge-NWHKs@CFC are shown in Figure S4 (Supporting Information), indicating that the absorption band for Ag-NPs is located at around 360 nm.

To optimize SERS performance, SERS activities of Ag-NPs@Ge-NWHKs@CFC with different $AgNO_3$ immersion durations were tested by using aqueous R6G solutions (10^{-6} M), as shown in Figure 4a. The SERS spectra demonstrate the characteristic peaks of R6G at 612 cm^{-1} (C–C–C ring in-plane bending mode), 775 cm^{-1} (C–C–C ring out-of-plane bending mode), and 1361 cm^{-1} (aromatic C–C stretching vibration mode), respectively.[45] The SERS peak intensities of R6G increase with the $AgNO_3$ immersion time prolonging for the first 9 mins and then decrease with further elongating the immersion time. As the $AgNO_3$ immersing duration increased from 3 mins to 9 mins, the Ag-NPs grows bigger and the gaps between nearby Ag-NPs decreased which generate the "hot spots" (Figure 3a-b), thus the intensity of the Raman peaks increased observably. When the immersing duration was further increased from 9 mins to 15 mins, the Ag-NPs became so large that they aggregated together to form blocky nanostructures which eliminate some "hot spots", thus decreasing the intensity of the Raman peaks. Therefore, about 9 mins of $AgNO_3$ immersion is the most appropriate duration for constructing the ultrasensitive SERS substrates.

To demonstrate the high sensitivity of the 3D flexible SERS substrates, SERS measurement was carried out with different concentrations of R6G. The spectral features of R6G can be identified clearly even at a concentration as low as 1 pM (shown in Figure 4b), verifying the high sensitivity of the Ag-NPs@Ge-NWHKs@CFC for SERS detection. Also, the average enhancement factor (EF) value for the Ag-NPs@Ge-NWHKs@CFC was estimated to be 1.05×10^{7} (see Part S6 in the Supporting Information for details), confirming the high sensitivity again.

To display the SERS signal reproducibility of the as-prepared 3D flexible SERS substrates, the SERS mapping of

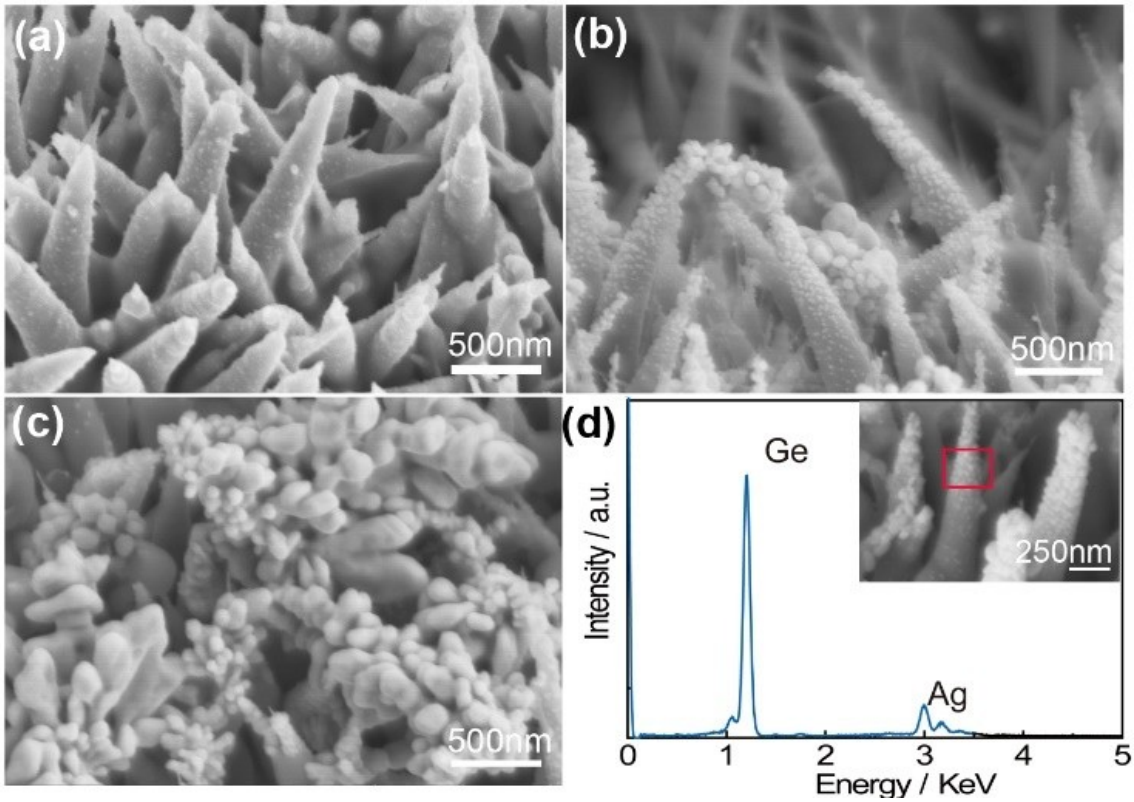

Figure 3. SEM images of the Ag-NPs@Ge-NWHKs with different $AgNO_3$ immersion durations of 3 min (a), 9 min (b) and 15 min (c). (d) EDS spectrum of the red rectangle area in the inserted SEM image of Ag-NPs@Ge-NWHKs with $AgNO_3$ immersion duration of 9 min.

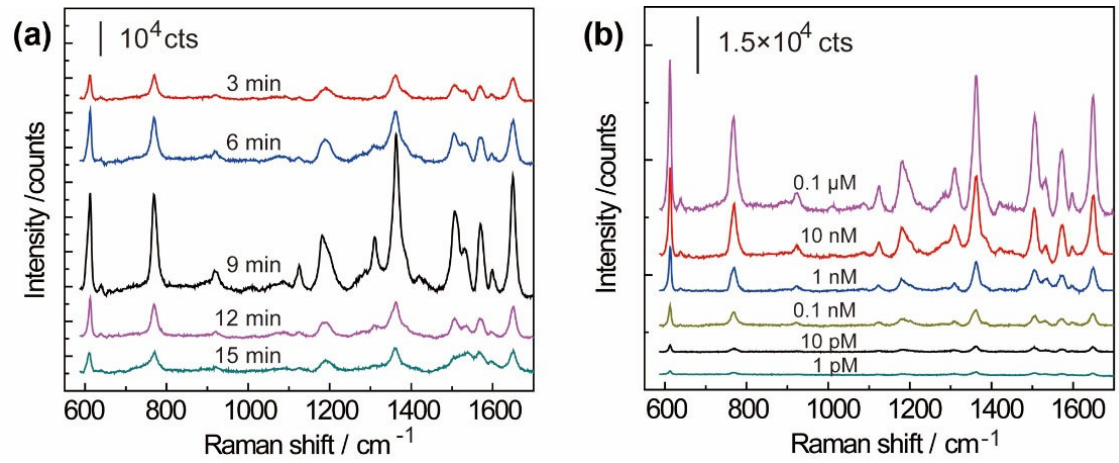

Figure 4. SERS sensitivity of the Ag-NPs@Ge-NWHKs@CFC to R6G. (a) SERS spectra of 10^{-6} M R6G adsorbed on the Ag-NPs@Ge-NWHKs@CFC fabricated under different $AgNO_3$ immersion durations. (b) SERS spectra of R6G with different concentrations adsorbed on the optimal Ag-NPs@Ge-NWHKs@CFC achieved by 9 min $AgNO_3$ immersion.

10^{-7} M p-mercaptobenzoic acid (p-MBA) taken from a 100× 100 μm^2 area on the Ag-NPs@Ge-NWHKs@CFC was measured, as shown in Figure 5a. The homogeneity of SERS signals of p-MBA collected at one hundred spots on the substrate were shown in Figure 5b, and the average relative standard deviation of the intensities of the peaks 1585 cm^{-1} is less than 10%. The relative standard deviation of 1361 cm^{-1} peak intensities of R6G taken from 25 substrates from different batches (shown in Figure S6, in the Supporting Information) was 20.7%. These results reveal the good signal reproducibility of Ag-NPs@Ge-NWHKs@CFC.

Comparing with the conventional rigid SERS substrates, the obtained 3D flexible SERS substrates are bendable and deformable (as shown in Figure S7), which is convenient for

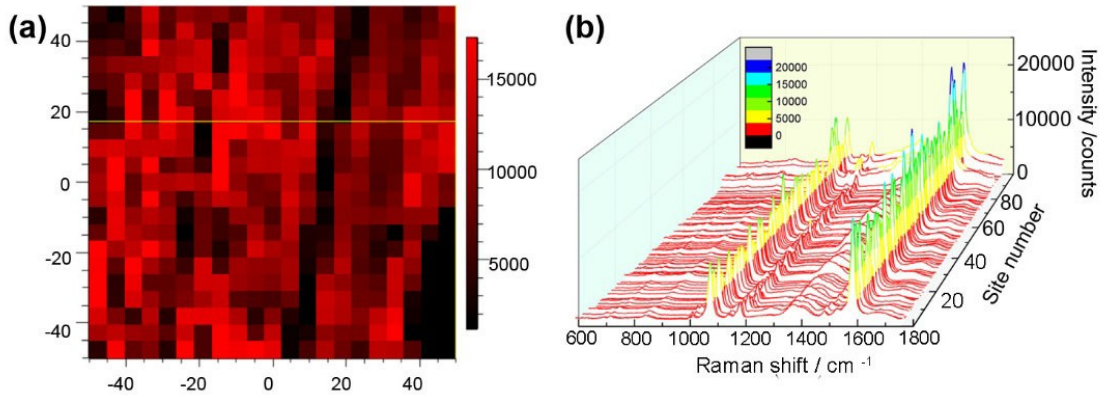

Figure 5. (a) A SERS intensity map (100 μm × 100 μm) of the 1585 cm^{-1} band of p-MBA observed from the Ag-NPs@Ge-NWHKs@CFC. (b) SERS spectra of 10^{-7} M p-MBA collected from 100 random spots on Ag-NPs@Ge-NWHKs@CFC.

different practical applications. Finally, to further explore the potential application of the as-fabricated SERS substrates, Ag-NPs@Ge-NWHKs@CFC were employed to detect thiram (a fungicide). Figure 6 shows the SERS spectra of thiram with different concentrations from 100 μM to 0.1 nM adsorbed on the Ag-NPs@Ge-NWHKs@CFC. It demonstrates that with a low concentration even down to 0.1 nM, the characteristic peaks of CN stretch (1512 cm^{-1}), the rocking CH_3 mode weakly coupled to the CN stretching mode (1382 cm^{-1}), the symmetric CH_3 deformation mode weakly coupled to the CN stretching mode (1143 cm^{-1}), and the SS stretching mode (561 cm^{-1}) of thiram can still be identified.[46–47] Therefore, the Ag-NPs@Ge-NWHKs@CFC can serve as effective SERS-substrates for the detection of toxic organic pollutants in the environment.

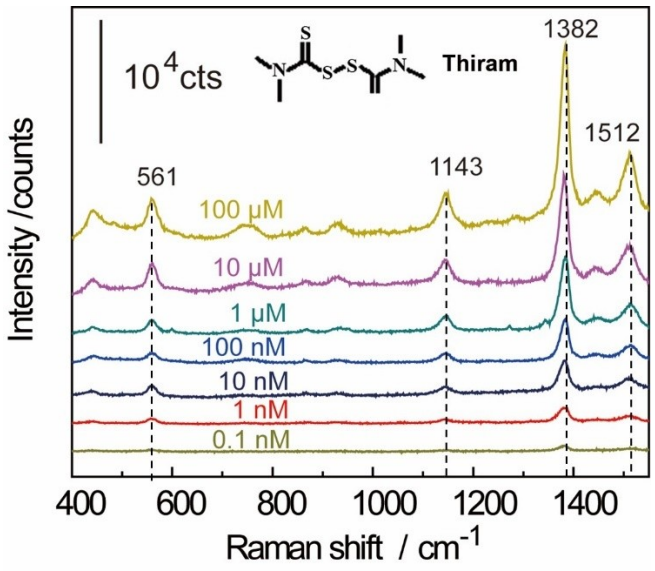

Figure 6. SERS spectra of thiram with different concentrations (from 100 μM to 0.1 nM) adsorbed on the optimal Ag-NPs@Ge-NWHKs@CFC. The inset shows the molecular structure of thiram.

3. Conclusion

In summary, 3D flexible SERS substrates of Ag-NPs@Ge-NWHKs@CFC were achieved *via* a combined process of CVD and galvanic displacement. Here, galvanic displacement is an easy and cost-effective method for Ag-NPs synthesis. The flocky Ge-NWHKs grafted on CFC with large surface area lead to a good Ag-NPs-carrying capacity, and thus high SERS sensitivity. The regular morphology of Ag-NPs@Ge-NWHKs@CFC guarantees reproducible SERS signal. In addition, trace thiram were recognized successfully by using the as-fabricated SERS substrates, showing its potential for rapid detection of organic pollutants in environment.

Supporting Information

This supporting information includes: experimental section, SEM image of Ge-NWHKs@CFC achieved without using GO, size distributions of Ag-NPs, high resolution SEM image of Ag-NPs@Ge-NWHKs, optical absorption spectrum of Ag-NPs@Ge-NWHKs@CFC, enhancement factor calculation, intensity distribution of SERS spectra of 25 Ag-NPs@Ge-NWHKs@CFC SERS substrates from different batches, photographs of Ge-NWHKs@CFC and SEM image of carbon fiber cluster.

Acknowledgements

This work was supported by the Natural Science Foundation of China (Grants 51632009, 21671192), Key Research Program of Frontier Sciences, the CAS/SAFEA International Partnership Program for Creative Research Teams, Anhui Provincial Natural Science Foundation for Distinguished Young Scholar (1808085 J12), CAS (Grant QYZDJ-SSW-SLH046), and German Research Foundation (DFG: LE 2249/5-1).

Conflict of Interest

The authors declare no conflict of interest.

Keywords: chemical vapor deposition · galvanic displacement · germanium nanowhiskers · surface plasmon resonance · silver nanoparticles

[1] M. J. Banholzer, J. E. Millstone, L. Qin, C. A. Mirkin, *Chem. Rev.* **2008**, *37*, 885–897.
[2] K. Kneipp, H. Kneipp, I. Itzkan, R. R. Dasari, M. S. Feld, *Chem. Rev.* **1999**, *99*, 2957–2976.
[3] S. Nie, S. R. Emory, *Science* **1997**, *275*,1102–1106.
[4] H. Abramczyk, B. Brozek-Pluska, *Chem. Rev.* **2013**, *113*, 5766–5781.
[5] Y. Wang, B. Yan, L. Chen, *Chem. Rev.* **2012**, *113*, 1391–1428.
[6] Y.-T. Long, J. J. Gooding, *ACS Sens.* **2016**, *1*, 963–963.
[7] E. S. Prikhozhdenko, D. N. Bratashov, D. A. Gorin, A. M. Yashchenok, *Nano Res.* **2018**, *11*, 4468–4488.
[8] J. J. Baumberg, T. A. Kelf, Y. Sugawara, S. Cintra, M. E. Abdelsalam, P. N. Bartlett, A. E. Russell, *Nano Lett.* **2005**, *5*, 2262–2267.
[9] Y. Fang, N.-H. Seong, D. D. Dlott, *Science* **2008**, *321*, 388–392.
[10] M. L. Pedano, S. Li, G. C. Schatz, C. A. Mirkin, *Angew. Chem. Int. Ed.* **2010**, *49*, 78–82.
[11] M. Rycenga, X. Xia, C. H. Moran, F. Zhou, D. Qin, Z.-Y. Li, Y. Xia, *Angew. Chem. Int. Ed.* **2011**, *50*, 5473–5477.
[12] M. Chen, I. Y. Phang, M. R. Lee, J. K. W. Yang, X. Y. Ling, *Langmuir* **2013**, *29*, 7061–7069.
[13] R. Que, M. Shao, S. Zhuo, C. Wen, S. Wang, S.-T. Lee, *Adv. Funct. Mater.* **2011**, *21*, 3337–3343.
[14] S. J. Lee, A. R. Morrill, M. Moskovits, *J. Am. Chem. Soc.* **2006**, *128*, 2200–2201.
[15] C. Zhang, S. Jiang, C. Yang, C. Li, Y. Huo, X. Liu, A. Liu, Q. Wei, S. Gao, X. Gao, B. Man, *Sci. Rep.* **2016**, *6*, 25243.
[16] S. Y. Lee, S.-H. Kim, M. P. Kim, H. C. Jeon, H. Kang, H. J. Kim, B. J. Kim, S.-M. Yang, *Chem. Mater.* **2013**, *25*, 2421–2426.
[17] J. Huang, F. Chen, Q. Zhang, Y. Zhan, D. Ma, K. Xu, Y. Zhao, *ACS Appl. Mater. Interfaces* **2015**, *7*, 5725–5735.
[18] M. Macias-Montero, R. Peláez, V. Rico, Z. Saghi, P. Midgley, C. Afonso, A. Gonzalez-Elipe, A. Borras, *ACS Appl. Mater. Interfaces* **2015**, *7*, 2331–2339.
[19] S. Cui, Z. Dai, Q. Tian, J. Liu, X. Xiao, C. Jiang, W. Wei, V. A. L. Roy, *J. Mater. Chem. C* **2016**, *4*, 6371–6379.
[20] J. Zhao, M. Sun, Z. Liu, B. Quan, C. Gu, J. Li, *Sci. Rep.* **2015**, *5*, 16019–26029.
[21] Q. Zhang, Y. H. Lee, I. Y. Phang, C. K. Lee, X. Y. Ling, *Small* **2014**, *10*, 2703–2711.
[22] J. Cai, J. Huang, M. Ge, J. Iocozzia, Z. Lin, K.-Q. Zhang, Y. Lai, *Small* **2017**, *13*, 1604240–1604252.
[23] X. Liu, J. Wang, L. Tang, L. Xie, Y. Ying, *Adv. Funct. Mater.* **2016**, *26*, 5515–5523.
[24] C. Zhang, P. Yi, L. Peng, X. Lai, J. Chen, M. Huang, J. Ni, *Sci. Rep.* **2017**, *7*, 39814–39823.
[25] S. K. Bhunia, L. Zeiri, J. Manna, S. Nandi, R. Jelinek, *ACS Appl. Mater. Interfaces* **2016**, *8*, 25637–25643.
[26] D. Cheng, H. Mantang, R. Jianhua, C. Guangming, W. Jihong, W. Xin, *Sens. Actuators B* **2018**, *270*, 508–517.
[27] W. Xin, J.-M. Yang, C. Li, M. S. Goorsky, L. Carlson, I. M. De Rosa, *ACS Appl. Mater. Interfaces* **2017**, *9*, 6246–6254.
[28] Z. Li, G. Meng, Q. Huang, X. Hu, X. He, H. Tang, Z. Wang, F. Li, *Small* **2015**, *11*, 5452–5459.
[29] H. Cui, S. Li, S. Deng, H. Chen, C. Wang, *ACS Sens.* **2017**, *2*, 386–393.
[30] O. Y. Dobrovets'ka, O. I. Kuntyi, G. I. Zozulya, I. V. Saldan, O. V. Reshetnyak, *Mater. Sci.* **2015**, *51*, 418–423.
[31] Z. Zhang, F. Liao, S. Ma, S. Gao, M. Shao, *Surf. Interface Anal.* **2015**, *47*, 398–402.
[32] M. Peng, J. Gao, P. Zhang, Y. Li, X. Sun, S.-T. Lee, *Chem. Mater.* **2011**, *23*, 3296–3301.
[33] T. Wang, F. Hu, E. Ikhile, F. Liao, Y. Li, M. Shao, *J. Mater. Chem. C* **2015**, *3*, 559–563.
[34] J. Liu, G. Meng, Z. Li, Z. Huang, X. Li, *Nanoscale* **2015**, *7*, 18218–18224.
[35] A. Martin, J. J. Wang, D. Iacopino, *RSC Adv.* **2014**, *4*, 20038.
[36] C. H. Lee, L. Tian, S. Singamaneni, *ACS Appl. Mater. Interfaces* **2010**, *2*, 3429–3435.
[37] D. Shruti, D. Bindesri, S. Dalal Alhatab, L. Christa Brosseau, *Analyst* **2018**, *143*, 4128–4135;
[38] W. X. Guo, C. Xu, X. Wang, S. H. Wang, C. F. Pan, C. J. Lin, Z. L. Wang, *J. Am. Chem. Soc.* **2012**, *134*, 4437–4441;
[39] L. Hao, H. Song, L. Zhang, X. Wan, Y. Tang, Y. Lv, *J. Colloid Interface Sci.* **2012**, *369*, 381–387.
[40] H. Wang, C. M. B. Holt, Z. Li, X. Tan, B. S. Amirkhiz, Z. Xu, B. C. Olsen, T. Stephenson, D. Mitlin, *Nano Res.* **2012**, *5*, 605–617.
[41] X. Li, G. Meng, Q. Xu, M. Kong, X. Zhu, Z. Chu, A.-P. Li, *Nano Lett.* **2011**, *11*, 1704–1709.
[42] X. Li, G. Meng, S. Qin, Q. Xu, Z. Chu, X. Zhu, M. Kong, A.-P. Li, *ACS Nano* **2011**, *6*, 831–836.
[43] C. Zhu, G. Meng, P. Zheng, Q. Huang, Z. Li, X. Hu, X. Wang, Z. Huang, F. Li, N. Wu, *Adv. Mater.* **2016**, *28*, 4871–4876.
[44] Z. Huang, G. Meng, Q. Huang, Y. Yang, C. Zhu, C. Tang, *Adv. Mater.* **2010**, *22*, 4136–4139.
[45] P. Hildebrandt, M. Stockburger, *J. Phys. Chem.* **1984**, *88*, 5935–5944;
[46] C. Yuan, R. Liu, S. Wang, G. Han, Z. Zhang, *J. Mater. Chem.* **2011**, *21*, 16264–16270.
[47] S. Kumar, P. Goel, J. P. Singh, *Sens. Actuators B* **2017**, *241*, 577–583.

Submitted: March 30, 2020
Accepted: June 10, 2020